

Multi-wavelength observations of the 2014 June 11 M3.9 flare: temporal and spatial characteristics

Damian J. Christian¹, David Kuridze^{2,3}, David B. Jess³, Menoa Yousefi¹ and Mihalis Mathioudakis³

¹ Department of Physics and Astronomy, California State University Northridge, Northridge, CA 91330, USA; *damian.christian@csun.edu*

² Institute of Mathematics, Physics and Computer Science, Aberystwyth University, Ceredigion, Cymru, SY23 3, UK

³ Astrophysics Research Center, School of Mathematics and Physics, Queen's University Belfast, Belfast BT7 INN, UK

Received 2018 month day; accepted 20xx month day

Abstract We present multi-wavelength observations of an M-class flare (M3.9) that occurred on 2014 June 11. Our observations were conducted with the Dunn Solar Telescope (DST), adaptive optics, the multi-camera system ROSA (Rapid Oscillations in Solar Atmosphere) and new HARDcam (Hydrogen-Alpha Rapid Dynamics) camera in various wavelengths, such as Ca II K, Mg I b₂ (at 5172.7 Å), and H α narrow-band, and G-band continuum filters. Images were re-constructed using the Kiepencheuer-Institut Speckle Interferometry Package (KISIP) code, to improve our image resolution. We observed intensity increases of \approx 120-150% in the Mg, Ca K and H α narrow band filters during the flare. Intensity increases for the flare observed in the SDO EUV channels were several times larger, and the GOES X-rays increased over a factor of 30 for the harder band. Only a modest delay is found between the onset of flare ribbons of a nearby sympathetic flare and the main flare ribbons observed in these narrow-band filters. The peak flare emission occurs within a few seconds for the Ca K, Mg, and H α bands. Time-distance techniques find propagation velocities of \approx 60 km/s and as high as 300 km/s for regions of the main flare ribbon. This result and delays and velocities observed with SDO (\approx 100 km/s) for different coronal heights agree well with the simple model of energy propagation versus height, although a more detailed model for the flaring solar atmosphere is needed. Future high time resolution observations of solar flares (such as those available with DKIST) are important for disentangling the detailed flare-physics.

Key words: magnetic reconnection– Sun: flares – Sun: atmosphere

1 INTRODUCTION

Solar flares vary in magnitude and frequency from rare, large, X-class flares, to common microflares and other sub-arcsecond explosive events. In flares, a rapid energy transfer occurs between the corona, chromosphere, and photosphere through non-thermal electron beams, radiation, conduction, Magnetoacoustic/Alfvén waves, and mass motions. The intermittent nature of the non-thermal electron beams can result in very rapid variations in chromospheric and coronal emission. These variations arise from a combination of energy/ionization imbalance and chromospheric condensation, and are determined by the intensity of the non-thermal energy flux deposited in the lower atmosphere. The chromospheric plasma is heated to very high temperatures (5–30 MK) creating an overpressure, leading to an expansion into the overlying atmosphere. This in turn results in blueshifts in upper chromosphere and transition region lines, a process known as chromospheric evaporation (Milligan et al. 2006; Pevtsov et al. 2007; Milligan et al. 2015). On the other hand, due to the upward and downward momentum balance there should be a downflowing pattern (condensation) as a back reaction of chromospheric evaporation, leading to redshifts of tens of kilometers per second in $H\alpha$ (Kuridze et al. 2015). Additionally, many flares are accompanied by white light emission. White light flare emission is observed in the near-UV and optical continuum, often appearing in transient footpoint regions (Neidig 1989; Isobe et al. 2007; Jess et al. 2008), and see reviews by Hudson et al. (2006); Hudson (2011), for example. The energy content of the white light component of a flare may actually exceed the soft X-ray component by a factor of 100 (Hudson 2011).

There are many open questions on the conditions in the photosphere and chromosphere pre-flare, and their response during the flare. Recent advances in solar imaging in both spatial and temporal resolution allow us to measure the response of the photosphere and chromosphere at multiple heights in the solar atmosphere. Thus, the morphology and temporal changes of the flare emission observed in different narrow-band filters (such as Ca K, Mg) promise to help constrain the detailed mechanisms of flare energy production and release, e.g. reviews by Fletcher et al. (2011); Hudson (2011). Lawrence et al. (1983), using observations in the Mg I b_2 line, found Mg flare kernels resembled white-light flare kernels, and associated the Mg emission with the impulsive flare phase. More recently, Bai et al. (2013) used Mg I b_2 to probe the poorly constrained chromospheric magnetic field.

In the present paper, we employ these new capabilities of higher spatial and temporal resolution of ground-based instrumentation and report on an M-class flare observed at several layers in the solar atmosphere. We observed an M3.9 flare observed on 2014 June 11 (SOL2014-06-11T21:03 UT), with the Rapid Oscillations of the Solar Atmosphere or (ROSA), HARDcam and CSUNcam instruments at the National Solar Observatory’s Dunn Solar Telescope. In Section 2 we present the ROSA and ground-based observations and data analysis, and inclusion of observations from NASA’s Solar Dynamic Observatory (SDO). In Section 3 we present results for the flare characteristics, and compare these to previous observations and discuss the flare propagation in simple models in Section 4. Lastly, in Section 5 we summarize our findings.

2 OBSERVATIONS

Our data were obtained with the Rapid Oscillations in the Solar Atmosphere (ROSA; Jess et al. 2010) (ROSA; Jess et al. 2010) camera system. ROSA is a synchronized, multi-camera high cadence solar imager installed on the Dunn Solar Telescope (DST) at the National Solar Observatory, Sacramento Peak, NM. The DST pointing was at S18.5E60.0, covering AR 12087 (at heliocentric coordinates, $-755''$, $-295''$). The observations sequence started at 19:20 UT, and continued until 21:31 UT, with a span of just over 2 hours and 11 minutes. The ROSA continuum channels recorded 30 fps and narrow-band Mg I b_2 filter was obtained at half of this data rate. The ROSA set-up used with a wider field of view than many previous studies, $\approx 2'$ giving a resolution of $0.12''$ per pixel or a 2-pixel diffraction-limited resolution of ≈ 173 km. ROSA was combined with the Hydrogen-Alpha Rapid Dynamics camera (HARDcam) (Jess et al. 2012) and CSUNcam (Grant et al. 2015), using $H\alpha$ and Ca II K (hereafter Ca K) filters at a frame rate of 30 fps, respectively. Central wavelengths and filter properties for the $H\alpha$ and Ca K are given in Jess et al. 2010. Interferometric Bidimensional Spectrometer (IBIS; Cavallini 2006; Reardon & Cavallini 2008) observations using the Na D_1 line were also obtain and have been presented by (Kuridze et al. 2016). The observations were obtained with high-order adaptive optics (Rimmele 2004) to correct wavefront deformations in real-time. Although, the overall seeing was poor at times and the observations hampered by clouds, we were able to measure the flare properties and perform speckle image reconstruction. The Kiepenheuer-Institut Speckle Interferometry Package (KISIP) speckle reconstruction algorithm (Wöger et al. 2008), was used on the images, with a 64 to 1 restoration. The Mg I b_2 (hereafter Mg) data was obtained with a cadence of 15.15 fps, and the reconstructed cadence is 4.22 seconds per image. The $H\alpha$ and Ca K data were obtained at 30.3 fps and both have a reconstructed cadence of 2.12 seconds per image. Our ground-based observations caught the M3.9 flare rising at $\sim 20:53$ UT and peaking near 20:57 UT, and the GOES X-ray bands measured the flare peak at $\sim 21:03$ UT. We show a sequence of flare images in the Ca K, Mg, $H\alpha$, and G-band in Figure 1. Flare light curves for all 3 bands were extracted in a $34' \times 26'$ region.

2.1 Solar Dynamic Observatory Observations

We further supplemented our ROSA observations with EUV data from the Atmospheric Imaging Assembly (AIA) on-board the Solar Dynamics Observatory (SDO; Lemen et al. 2012) and magnetic information from

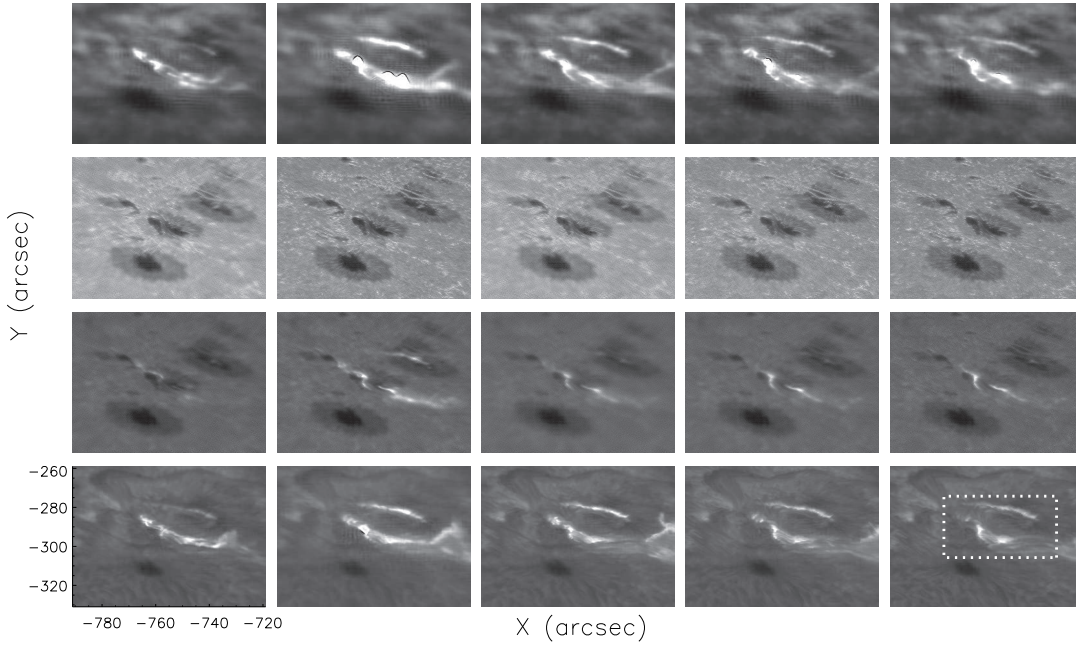


Fig. 1: Image sequence from ground-based observations from ROSA, HaRDcam and CSUNcam spanning the 2014 June 11 M3.9 class flare peak. Filters from top to bottom are: Ca K, G-band, Mg I b_2 and $H\alpha$. The extraction region for flare light curves is indicated in the lower right panel for $H\alpha$.

the Helioseismic and Magnetic Imager (HMI; Scherrer et al. 2012; Schou et al. 2012). The AIA instrument images the entire solar disk in 10 different channels, incorporating a two-pixel spatial resolution of $1.2''$ (≈ 900 km for the AIA’s PSF) and a cadence of 12 sec for the EUV channels and 24 sec for the 1600 and 1700 Å channels. Here, we selected 5 EUV datasets spanning 20:30 – 22:00 UT on 2014 June 11, consisting of 445 images in each of the 193, 211, & 304 Å AIA channels (94 and 131 Å channels were saturated and are not included in the present work), and 222 images for the 1600 and 1700 Å channels. The SDO observations caught the M3.9 flare starting at approximately 20:53 UT and the subsequent brightening peaking at near 20:57 for the cooler SDO channel and $\sim 21:06$ UT for the hotter channels. Light curve for the different SDO channels were extracted in a $120'' \times 90''$ region. Sample SDO images along with our Mg and $H\alpha$ bands are shown in Figure 2. We also obtained the HMI line-of-sight (LOS) magnetograms from 20:48 and 21:12 UT, before and after the flare, respectively. The HMI images were aligned and degraded to the AIA resolution with hmi_prep.

3 RESULTS

3.1 Flare Properties

Our multi-wavelength observations of AR 12087 detected an M3.9 flare on 2014 June 11. The GOES soft (1–8 Å) and hard (0.5–4.0 Å) X-rays peaked at 21:03 UT and rose factors of 15 and 33 over the quiescent emission, respectively. The flare in the ROSA Mg I b_2 light curve rose a factor of 1.24 over the quiescent

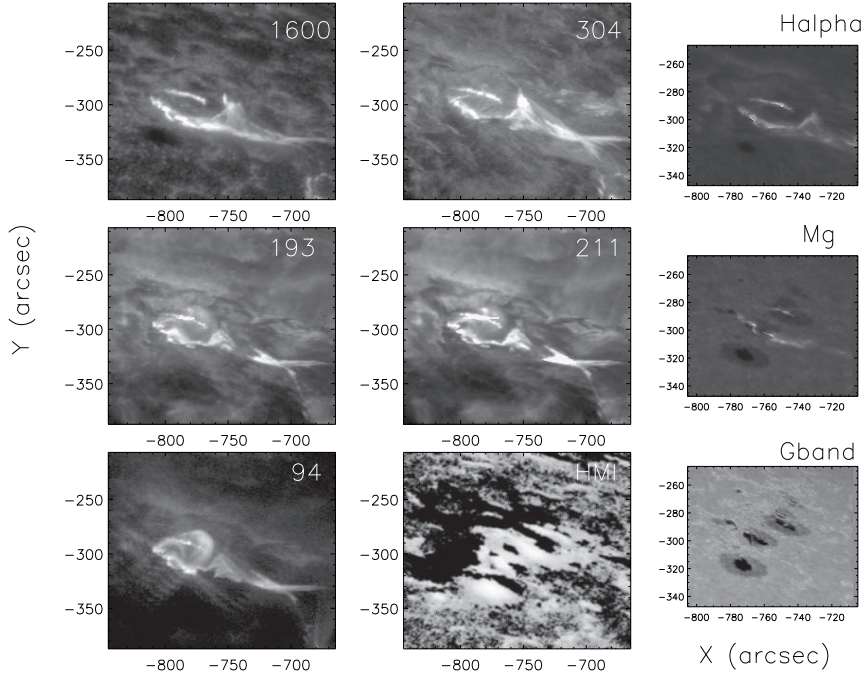


Fig. 2: SDO/AIA flare images in 5 different bands near the flare peak, along with our HARDCam $H\alpha$, and ROSA G-band and Mg observations in the right column. The HMI LOS magnetogram is also shown in the lower middle panel (see text).

emission and peaked near 20:56:51 UT. The Ca K and $H\alpha$ light curves increased a factor of 1.55 and 1.5 over their pre-flare, quiescent emission, respectively. In Figure 3 we compare the narrow-band filter data to that obtained from the GOES X-ray satellite. The rise time for the Mg flare was ~ 105 sec, with a decay times of the narrow band filters exceeding 30 minutes and the overall emission stays larger than the pre-flare quiescent emission for the remaining time of our observations. The GOES peak for our M3.9 flares is $3.9 \times 10^{-5} W/m^2$. This works out to a total energy in the 1.0 to 8.0 band of 1.1×10^{29} ergs for the 17 minute flare duration. We summarize the flare parameters in different bands in Table 1 extracted from the regions noted in Section 2.

3.2 Flare Morphology

The flare emerged in the Ca K, Mg and $H\alpha$ images as 2 separate flare ribbons that evolved into the lower longer flare ribbon (“main”) with a length of about 25 Mm and a smaller sympathetic flare ribbon about 18 Mm long separated by 7 to 10 Mm above. We looked for differences in the flare properties across the flare ribbons in different regions. We show the flare light curves extracted all three bands from these different regions in Figure 4a along with the flare image for $H\alpha$. There was essentially no difference in the rise times between the east and west regions surrounding the lower main flare ribbon. Moving from east to west along the lower flare ribbon find similar rise times, with the largest peak from region labeled box “5”. Although in the main flare ribbons, the left region (box labeled “0”) rises about 30 seconds before the emission from the

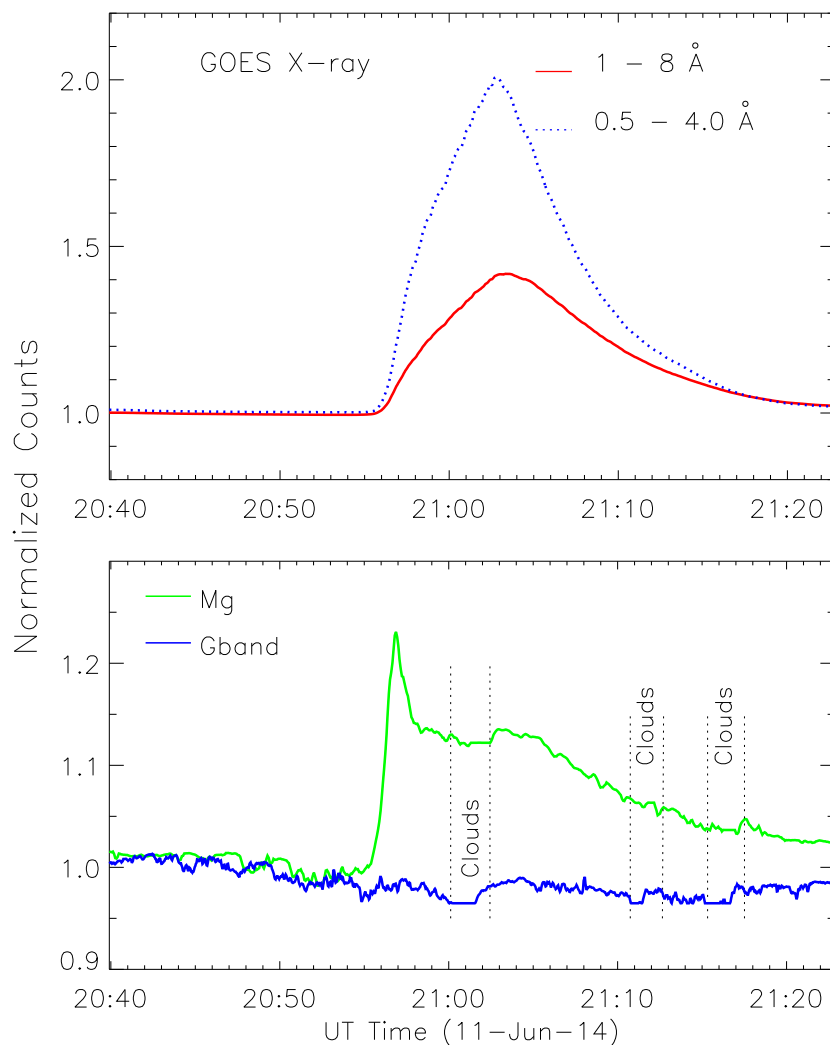


Fig. 3: Sample light curves for the 2014 June 11 M3.9 flare as a function UT times on 2014 June 11 . The top panel shows both the GOES soft X-ray channels with the $0.5 - 4 \text{ \AA}$ displayed in blue and the $1.0 - 8.0 \text{ \AA}$ in red. The lower panel shows the ROSA Mg (green) and G-band (blue) light curves. Intervals disrupted by clouds are indicated in the lower panel.

upper (sympathetic) flare ribbon (labeled box “7”). The ribbon appears to be erupting along the east-to-west direction, but not in a linear fashion that makes a propagation velocity easily calculated. The more eastward and westward regions showed a more gradual increase than the central regions and only reached a levels ≈ 1.5 times higher than the quiescent emission, about 40% lower than the flare peaks for the central regions of the main flare ribbon. In the next section we investigate velocities using time-distance techniques.

Table 1: Light Curve Results

λ	Peak (UT)	Rise (min)	Decay (min)	Peak/Quiescent
G-band	No Flare
Ca K	20:56:49	~ 1.5	> 30	1.55
Mg	20:56:51	~ 1.7	~ 30	1.24
H α	20:56:51	~ 1.5	> 35	1.50
SDO 304	20:56:43	~ 2	~ 46	4.3
SDO 193	20:56:43	~ 7	~ 28	3.4
SDO 211 ¹	20:58:01	~ 2	1.4	1.66
	21:06:39	~ 11	~ 40	2.0
SDO 1600	20:56:31	~ 31	~ 28	4.6
Hard X-Ray	21:03	~ 10	~ 17	33
Soft X-Ray	21:03	~ 10	~ 19	15

¹Two flare peaks are observed in the 211 Å band.

3.3 Velocities

We attempted to measure the propagation speed of the erupting ribbons in the photosphere and chromosphere during the flare’s evolution in the narrow filter bands (Ca K, Mg and H α) using time-distance techniques. Although it is difficult to distinguish a propagation velocity across the main flare ribbon, we find a velocity of 250 km/s (shown in Figure 4b) for both H α and Ca K. The expanding region at the western end of the main ribbon shows a velocity of 60 km/s with smaller features moving as fast as 300 km/s. Similar velocities were found for the Mg band, but were difficult to derive based on its longer cadence, and lower contrast and signal-to-noise.

4 DISCUSSION

We investigated the properties of an M3.9 flare observing in multiple narrow and continuum band filters and supplemented with EUV imaging data from SDO. Many issues still remain in our understanding of the details of flare physics (densities, temperatures, and magnetic field configurations) that can only be derived from simultaneous observations at high temporal resolution of many layers of the solar atmosphere.

4.1 Flare Properties

We observed intensity increases ≈ 120 to 150% in the Mg, Ca K and H α narrow band filters during the flare. Intensity increases for the flare observed in the SDO EUV were several times larger and the GOES X-rays increased a factor of 15 in the soft X-ray band and over a factor of 30 for the harder band. These observed intensity increases in our narrow band filter are slightly lower than those of previous studies (Keys et al. 2011) and may indicate the majority of the flare emission is at hotter temperatures, as observed by the factor of 4–5 times increase observed with SDO.

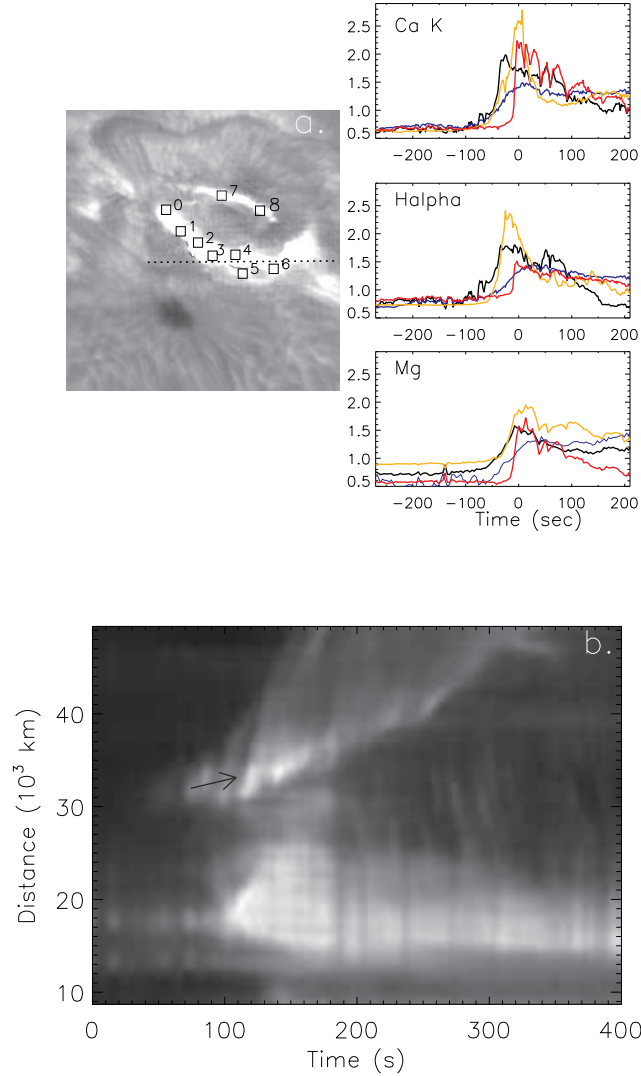


Fig. 4: Shown are comparisons of the $H\alpha$, Ca K and Mg light curves extracted from different spatial regions during the M3.9 flare and a time-distance plot for $H\alpha$. a. (upper panels) The regions the light curves were extracted from are shown in in the left upper panel for $H\alpha$ only. The dashed horizontal line shows where the time-distance plot was taken. The upper left panels show light curves extracted from four selected regions (0 - black, 3-, 5, 7 - red, for ease of presentation), from top to bottom for: Ca K, $H\alpha$, and Mg, respectively. b. (lower panel) Time-distance plot showing motion along the flare ribbon and western region for $H\alpha$ (see text).

4.2 Flare Morphology

Our observations covered nearly 1 hour before the flare and we are able to observe the detailed morphology of the flare ribbons change on a timescale of seconds. There appear to be two flare ribbons, a lower larger “main” ribbon and an upper smaller region observed in our Ca K, Mg, and $H\alpha$ flare emission. These ribbons of our flare appear to be related and occur within 30 seconds of each other. We find a length of ≈ 25 Mm for the lower main flare ribbon in $H\alpha$ and Ca K, and Mg bands. The flare ribbons are very similar to that of

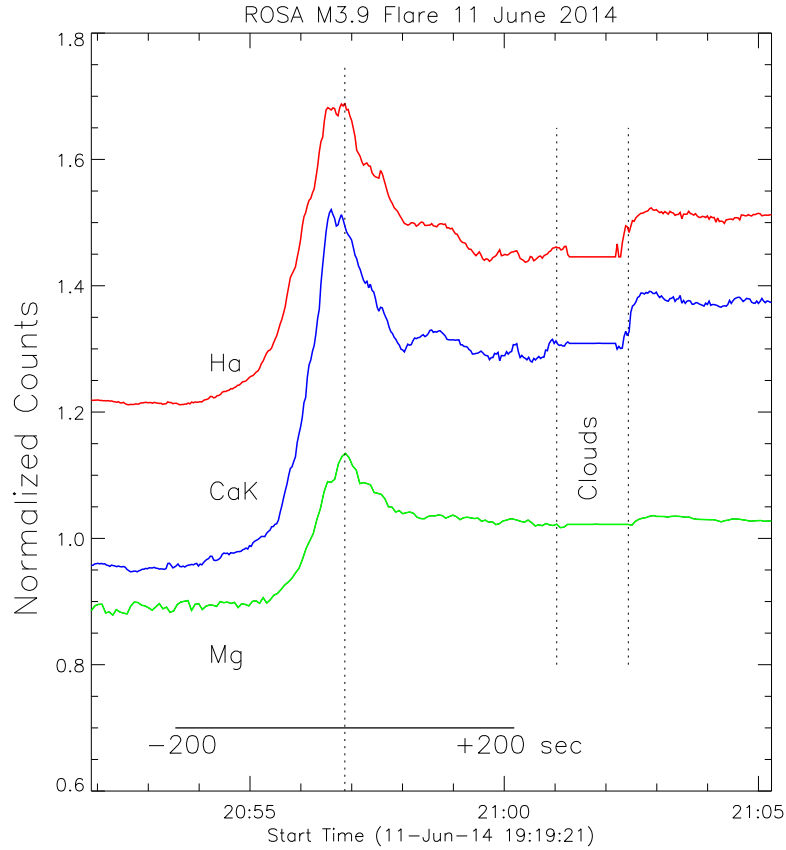


Fig. 5: Light curves for different filters for the M3.9 flare. From top to bottom are the $H\alpha$, Ca K, and Mg based plotted in normalized counts (Mg is offset for ease of presentation). No significant delay in the flare peak times is observed between the Mg, Ca K and $H\alpha$ and Mg peaks and is indicated with a vertical dashed line in addition to intervals affected by clouds (see text).

white-light flare emitting regions (Svestka 1976; Dodson-Prince & Bruzek 1977) and can be compared in our Mg band to the Mg I b_2 observations of Lawrence et al. (1983), albeit the 1983 data are at lower spatial resolution.

4.3 Velocities

We find almost no difference in the flare's rise times for light curves extracted from regions across the main flare ribbon (Figure 4a) and velocities when comparing various physical regions of the flare using time-distance plots. Also, the rise and decay times between these regions are all very similar (see Figure 4a). The

peaks of the Mg, Ca K and H α emission are all within ≈ 2 seconds (Figure 5). Typical formation heights for Ca K and H α are 1300 km and 1500 km, respectively (VAL- Vernazza et al. 1981; FAL90- Fontenla et al. 1990). This would imply a propagation velocity of about 100 km/s between these 2 layers, but the uncertainties are large. However, it is curious that the Mg emission, which forms near 700 km (Schmieder 1979); occurs within seconds of the Ca K and H α emission peaks. This implies during the flare this emission could either be being formed at greater heights, similar to the Ca K and H α formation heights. This would be in agreement for flaring models presented by Mauas et al. (1990). This discrepancy may also result from the width of the Mg filter being sensitive to emission at several depths, and we also realize the formation height of chromospheric spectral lines during the flare are significantly different then when comparing to the VAL model for the quiet Sun.

Similar calculations can be carried out for the SDO data, although we caution that the 12 sec cadence of the AIA EUV channels and the 24 sec cadence of the 1600 Å channel makes the uncertainties in these velocities large, and the SDO filters AIA filters are broadband, capturing emissions from multi-thermal layers with uncertain formation heights. However it gives us a ball-park estimate for propagation velocities to compare with the photosphere and chromosphere. We use Reznikova et al. (2012) for SDO's formation heights and find velocities consistent with ~ 100 km/s between emission observed in the SDO 304 & 1600 Å channels (formation heights for SDO 304 & 1600 Å are 2200 km and 500 km, respectively), and for propagation between the 304 and SDO 171 ($\Delta H = 1000$ km). We can also compare our photospheric and chromospheric measurements to those of the transition region and corona as measured by SDO. We can compare the delay between Ca K and the SDO 304 Å band. These 2 layers have a height difference of 900 km for the standard VAL model and this results in a velocity of 75 km/s. If the Ca K formation height is much lower, i.e. 500 km, then the propagation velocity is larger, at ≈ 140 km/s, a slightly higher velocity than a typical M-class flare, and similar to velocities found for other SDO channels. Again we caution the quiet-Sun VAL model is not applicable for the formation heights of chromospheric spectral lines during the flare. The colder SDO channel (SDO 304 with about 50,000 K) had a longer decay time than a hot SDO channel (SDO 193 with about 1 million K), and as we would have expected the SDO 193 peaks later (about 8 seconds) than SDO 304, since SDO 193 covers the coronal region and SDO 304 the chromosphere. In Figures 7 we illustrate the light curves for several SDO channels along with our ground-based narrow band channels. The second peak of the SDO 211 Å channel ($\approx 2 \times 10^6$ K), and the hotter channels (94 and 131 Å, not shown) peak over 8 minutes later than the than the cooler SDO channels (e.g. 193, 304 Å) similar to what was observed by Cheng et al. (2015) for a two-ribbon M-class flare and in a sample of flares presented by Aschwanden & Shimizu (2013).

5 SUMMARY AND CONCLUSIONS

We have presented multi-wavelength observations of the 2014 June 11 M3.9 flare. We observed intensity increases ≈ 120 -150% in the Mg, Ca K and H α narrow band filters during the flare. Intensity increases for the flare observed in the SDO EUV were several times larger (≈ 4 times for 304 Å with $T \approx 50,000$ K),

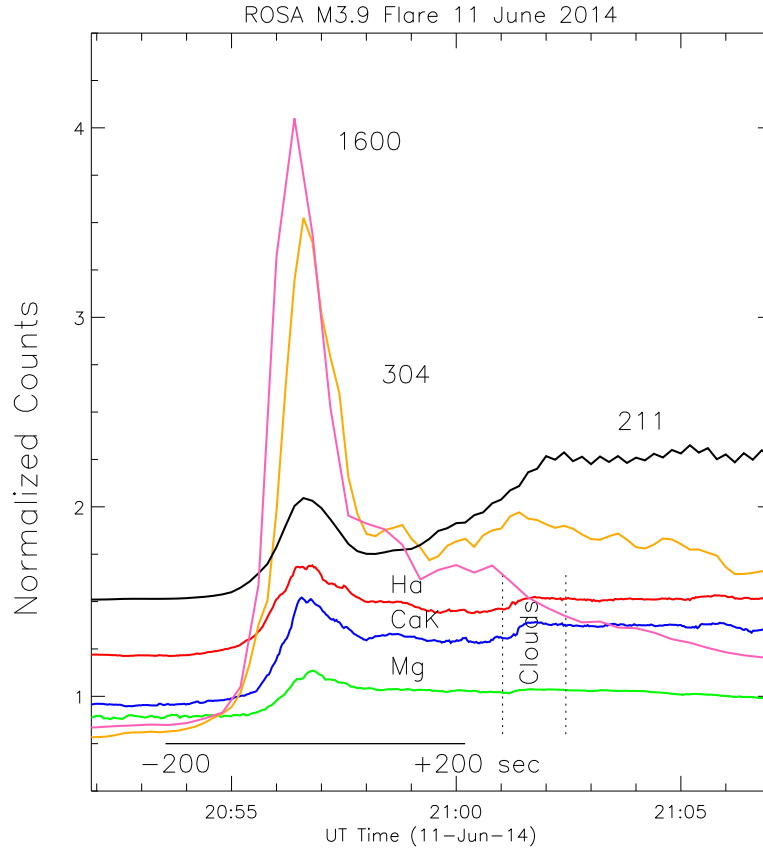


Fig. 6: Shown are the light curves for the cooler SDO channels (211, 304, & 1600 Å) with our CaK (blue), Mg (green) and H α (red) narrow-band filter data. Individual light curves are normalized by their average counts and are offset for ease of presentation. The SDO AIA channels shown are: 211 (black), 304 (orange), and 1600 Å (pink).

and the GOES X-rays increased over a factors of 15 and 33 for the soft and hard bands, respectively. The flare morphology observed in these narrow-band filters shows a main flare ribbon and a sympathetic flare ribbon about 7 to 10 Mm away. Only modest delays are found between the onset of emission across the main flare ribbon and upto 30 seconds between the main flare regions and of the nearby sympathetic flare (upper region). The peak flare emission occurs within a few seconds for the Ca K, Mg, and H α bands. Time-distance techniques find propagation velocities of ≈ 60 km/s and as high as 300 km/s for regions in the main flare ribbon. Propagation velocities between the chromosphere and coronal layers, although uncertain, are found to be as large as ≈ 100 km/s. These results and delays and velocities for different

coronal heights observed with SDO are consistent with this velocity, and agree well with the simple model of energy propagation versus height, although a more detailed model for the flaring solar atmosphere is needed. Future high time resolution observations of solar flares are important for disentangling the detailed flare-physics.

Acknowledgements We thank the NSO Dunn Solar Telescope staff, including Doug Gilliam for their excellent support for this project, and we dedicate this paper to the late Michael Bradford who's keen eye pointed out this solar flare.

References

- Aschwanden, M., Shimizu, T. 2013, *ApJ*, 776, 132
- Bai, X.-Y., Deng, Y.-Y., Su, J.-T., Wang, G.-P. 2013, *Res. in Astronomy & Astrophysics*, 14, 193
- Cavallini, F., 2006, *Solar Physics*, 236, 415
- Cheng, X., Hai, Q., Ding, M. D., Liu, K., Chen, P. F., Fabg, C., Liu, Y.D. 2015, *ApJ*, 809, 46
- Dodson-Prince, H. W., & Bruzek, A. 1977, in *Illustrated Glossary for Solar and Solar-Terrestrial Physics*, ed. A. Bruzek & C. J. Durrant (Dordrecht: Reidel), 81
- Fletcher, L., Dennis, B. R., Hudson, H. S. et al. 2011, *SSRv*, 59, 19
- Fontenla, J. M., Avrett, E., & Loeser, R. 1990, *ApJ*, 355, 700 (FAL90)
- Grant, S. D., Jess, D. B., Moreels, M. G. et al. 2015, *ApJ*, 806, 132
- Hudson, H. S., Wolfson, C. J., Metcalf, T. R. 2006, *Sol. Phy.* 234, 79
- Hudson, H. 2011, *Space Sci. Rev.*, 158, 5
- Isobe, H., Kubo, M., Minoshima, T. et al. 2007, *PASJ*, 595, 807
- Jess, D. B., Mathioudakis, M., Crockett, P. J., Keenan, F. P. 2008, *ApJ*, 688, 119
- Jess, D. B., Mathioudakis, M., Christian, D. J., Keenan, F. P., Ryans, R. S. I., Crockett, P. J. 2010, *Solar Phys.*, 261, 363
- Jess, D. B., De Moortel, I., Mathioudakis, M., Christian, D. J., Reardon, K. P., Keys, P. H., Keenan, F. P. 2012, *ApJ*, 757, 160
- Keys, H. P., Jess, B. D., Mathioudakis, M., Keenan, F. P. 2011, *A&A*, 529, 127
- Kuridze, D., Mathioudakis, M., Simões, P. J. A. et al. 2015, *ApJ*, 813, 125
- Kuridze, D., Mathioudakis, M., Christian et al. 2016, *ApJ*, 832, 147
- Lawrence, K. J., Chapman, A. G., Herzog, D. A. 1983, *Solar Physics*, 89, 341
- Lemen, J. R., Title, A. M., Akin, D. J., et al. 2012, *Sol. Phys.*, 275, 17
- Mauas, P. J. D., Machado, M.E., Avrett, E. H. 1990, *ApJ*, 360, 715
- Milligan, R. O. et al. 2006, *ApJL*, 638, 117
- Milligan, R. O. 2015, *Sol. Phys.*, 290, 3399
- Neidig, D. F. 1989, *Solar Phys.*, 121, 261
- Pevtsov, A.A., Balasubramaniam, K. S., Hock, Rachel A. 2007, *Advances in Space Research*, 39, 1781
- Reardon, K.P., Cavallini, F. 2008 *A&A*, 481, 897

- Reznikova, V. E., Shibasaki, K., Sych, R. A., Nakariakov, V. M. 2012, *ApJ*, 746, 119
- Rimmele, T. R., 2004, *Proc. SPIE*, 5490, 34
- Scherrer, P. H., Schou, J., Bush, R. I., Kosovichev, A. G. et al. 2012, *Sol. Phys.*, 275, 207
- Schmieder, B. 1979, *Astronomy and Astrophysics*, 74, 273
- Schou, J., Scherrer, P. H., Bush, R. I., et al. 2012, *Sol. Phys.*, 275, 229
- Svestka, Z. 1976, *Solar Flares* (Berlin: Springer)
- Vernazza, J. E., Avrett, E. H., & Loeser, R. 1981, *ApJS*, 45, 635 (VAL)
- Wöger, F., von der Lhe, O., Reardon, K. 2008, *A&A*, 488, 375